

Ultimate Quantum Sensitivity in the Estimation of the Delay between two Interfering Photons through Frequency-Resolving Sampling

Danilo Triggiani^{1,*}, Giorgos Psaroudis¹, and Vincenzo Tamma^{1,2,†}

¹*School of Mathematics and Physics, University of Portsmouth, Portsmouth PO1 3QL, United Kingdom*

²*Institute of Cosmology and Gravitation, University of Portsmouth, Portsmouth PO1 3FX, United Kingdom*

(Received 21 June 2022; revised 1 February 2023; accepted 21 March 2023; published 24 April 2023)

We demonstrate the ultimate sensitivity allowed by quantum physics in the estimation of the time delay between two photons by measuring their interference at a beam splitter through frequency-resolving sampling measurements. This sensitivity can be increased quadratically by decreasing the photonic temporal bandwidth even at values smaller than the time delay when standard two-photon interferometers become inoperable and without adapting the path of the reference photon, nor the need of time-resolving detectors with an unfeasible high resolution. Applications can range from the more feasible imaging of nanostructures, including biological samples, and nanomaterial surfaces to quantum enhanced estimation based on frequency-resolved boson sampling in optical networks.

DOI: 10.1103/PhysRevApplied.19.044068

Photons manifest unique quantum properties that might appear odd and counter intuitive from a classical standpoint. A paradigmatic example of this unusual behavior is given by the interference of two identical photons after impinging separately at the two faces of a balanced beam splitter, as the two photons always end up together in one of the two output arms of the beam splitter [1–8]. This tendency of the photons to “bunch” together arises from the lack of information on which path the two photons undertake when interfering at the beam splitter. Such interference phenomenon is sensitive to the differences between the physical parameters associated with the two photons. This has motivated estimation schemes for high-precision measurements of the two-photon time delay [1,9–11], or the state of polarization of the photons [12]. Remarkably, the estimation of time intervals has achieved in this way precisions ranging from subpicoseconds [1] up to the attoseconds regime [9]. In particular, the employment of notions borrowed from estimation theory and the subsequent study of the Fisher information [13,14]—a way to quantify the ultimate amount of information that can be obtained about an unknown parameter with a given estimation scheme—have recently allowed for a further

boost in the levels of precision achievable [9–11,15]. On the other hand, these analyses also show that the sensitivity of schemes based purely on the observation of the coincidence and bunching statistic is highly dependent on how much the two photons differ from each other in the parameter to estimate, such as their relative time delay [1–9]. In particular, such two-photon interference techniques become insensitive to photonic time delays beyond the temporal bandwidth of the photons [1–9].

A different approach with respect to standard two-photon interference takes advantage of current detectors capable of resolving inner-mode variables of the photons, such as their time of arrival [15–20] or their frequencies [21–23]. Indeed, one can exploit the quantum beating, i.e., the oscillations in the count of coincidence and bunching events of two photons as a function of the detection times or the detected frequencies, to infer the value of the frequency shift or the time delay of the two photons, respectively [16,17,24,25]. Furthermore, differently from nonresolved two-photon interference (i.e., standard interferometry performed without resolving the photonic inner-mode variables), quantum beating can be observed even in the case of negligible overlap in the time or frequency domain between the photonic wave packets impinging at the beam splitter. However, although a quantum advantage for the inner-mode variables interference of independent photons has already been demonstrated from a computational point of view [26–28], the ultimate precision of such a technique from a metrological perspective is yet not known. This motivates the following important questions pertinent to the development of high-precision quantum sensing technologies, such as feasible observation and

*danilo.triggiani@port.ac.uk

†vincenzo.tamma@port.ac.uk

Published by the American Physical Society under the terms of the [Creative Commons Attribution 4.0 International license](#). Further distribution of this work must maintain attribution to the author(s) and the published article's title, journal citation, and DOI.

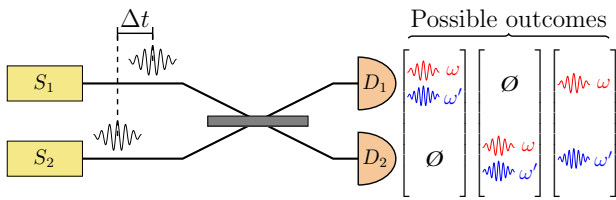


FIG. 1. Scheme of the interferometric setup. Two independent photons in the state in Eq. (1) with identical frequency distributions are produced by independent sources S_1 and S_2 with a given degree of indistinguishability η deriving from nontemporal properties (e.g., different polarizations). After impinging onto the two faces of a balanced beam splitter with an unknown time delay Δt , the two photons are eventually observed by the frequency-resolving detectors D_1 and D_2 . At each experimental run, a sample (ω, ω', X) from the output probability distribution in Eq. (3) is observed, where ω and ω' are the random values of the frequencies of the detected photons and $X = B, C$ specifies if it is a bunching (B) or a coincidence (C) event.

imaging of nanomaterials or nanostructures in biological samples [9]. Is there a quantum metrological advantage arising from the inner-mode variables quantum interference of photons? If yes, is it possible to quantify such an advantage in terms of the ultimate precision fundamentally achievable? How does such an advantage depend on the value of the parameter to estimate?

In this work we demonstrate the ultimate precision achievable in the estimation of time delays between independent photons with the same frequency distribution, interfering at a balanced beam splitter, and detected at the output with frequency-resolving detectors, as described in Fig. 1. We show that the measurement scheme proposed is optimal for identical photons with an arbitrary time delay. When instead a nonvanishing distinguishability between the two photons in any nontemporal property (e.g., polarizations) is present, the quantum advantage is still retained, even if such nontemporal distinguishability is not “erased” at the detectors by suitable measurements. In particular, we demonstrate that this scheme is effective also in the regime of photonic temporal bandwidth much smaller than their temporal delay, a regime in which nonresolving two-photon interferometry fails. This is a particularly interesting feature since, as we show, it allows us to employ extremely short photons, which have the largest sensitivity in the estimation of time delays, without the need of fine tuning the reference path of the interferometer with a precision comparable with the temporal bandwidth of the photons. We finally perform a numerical simulation showing how the ultimate precision assessed by the Fisher information we evaluate can be practically achieved with a feasible number of iterations of the experiment.

I. EXPERIMENTAL SETUP

The quantum state of the two independent photons before impinging on the beam splitter is (see Fig. 1)

$$|\psi\rangle = \int_{\mathbb{R}} d\omega_1 \xi_1(\omega_1) (\eta \hat{a}_{1,\omega_1}^\dagger + \sqrt{1 - \eta^2} \hat{b}_{1,\omega_1}^\dagger) |vac\rangle \\ \otimes \int_{\mathbb{R}} d\omega_2 \xi_2(\omega_2) \hat{a}_{2,\omega_2}^\dagger |vac\rangle, \quad (1)$$

where $\xi_i(\omega) = \bar{\xi}(\omega) e^{-i\omega t_i}$ is the frequency probability amplitude of the photon injected in the i th channel, with $i = 1, 2$ and $|\xi_1(\omega)| = |\xi_2(\omega)| \equiv \bar{\xi}(\omega)$ (photons with the same spectra), and t_i is the time of incidence of the i th photon on the beam splitter. The quantity $\Delta t = t_2 - t_1$ is thus the unknown delay to be measured. For a given frequency ω and spatial channel i , the commuting creation operators $\hat{a}_{i,\omega}^\dagger$ and $\hat{b}_{i,\omega}^\dagger$ denote orthogonal modes in any given additional degree of freedom, such as polarization or inner spatial modes: for $\eta = 1$, the two photons differ only in their injection times, while for $0 \leq \eta < 1$, a further distinction between the states of the two photons arises (e.g., they can be in different polarizations, where $\eta = 0$ is the limit case of orthogonal polarizations).

In our model, at each repetition of the experiment, the photons are randomly observed at either of the output ports of the balanced beam splitter. Simultaneously, their frequencies are measured at all possible random values within their frequency distribution $|\xi(\omega)|^2$ (with a given spectral bandwidth σ), with high enough resolution $\delta\omega$ so that their distinguishability in time is erased, i.e., for Gaussian spectra [21],

$$\delta\omega \ll \frac{1}{|\Delta t|} \quad \text{and} \quad \delta\omega \ll \sigma. \quad (2)$$

Noticeably, the second condition on $\delta\omega$ in Eq. (2) is weaker than the former in the regime of highest precision, which we show to be for large σ . For imperfect detectors able to detect an incoming photon with a finite probability $\gamma < 1$,

$$P_\eta(\omega, \omega', X) = \gamma^2 \bar{\xi}(\omega)^2 \bar{\xi}(\omega')^2 \\ \times \{1 + \alpha(X) \eta^2 \cos[(\omega - \omega') \Delta t]\}, \quad (3)$$

with $X = B, C$, $\alpha(B) = 1$ and $\alpha(C) = -1$, represents the probability of the sample outcome (ω, ω', X) of a single iteration of the experiment, in which the two photons either bunch in the same channel ($X = B$) or end up in different channels ($X = C$) with random frequency values ω and ω' , up to a factor $\delta\omega^2$ due to the resolution of the detectors (see Appendix B). Expectedly, the probability in Eq. (3) manifests quantum beats with a period inversely proportional to the photonic time delay Δt .

The experiment thus consists in sampling from the output probability distribution in Eq. (3) the outcomes

(ω, ω', X) , without spectral filtering at specific frequencies (see Appendix D). Therefore, similarly to boson sampling [26–28], the output probability distribution does not need to be experimentally reproduced avoiding therefore the need of a large number of experimental runs. Indeed, we show that, for photons with a Gaussian frequency distribution, it is enough to observe < 1000 samples, and, thus, photonic pairs, to achieve unbiasedness and optimal precision (see Appendix D).

II. BOUNDS ON THE PRECISION

To fully analyze the precision achievable with our setup in Fig. 1, we evaluate the bound on the variance $\text{Var}[\Delta t]$ of any unbiased estimator $\widetilde{\Delta t}$ associated with our scheme, given by the Cramér-Rao bound [13,14], and compare it with the smallest variance achievable with any measurement scheme, given by the quantum Cramér-Rao bound [29,30]. These bounds are related by the chain of inequalities

$$\text{Var}[\widetilde{\Delta t}] \geq \frac{1}{NF(\Delta t)} \geq \frac{1}{NH(\Delta t)}, \quad (4)$$

where N is the number of repetitions of the measurement, $F(\Delta t)$ is the Fisher information associated with the frequency-resolving estimation scheme [13,14], and $H(\Delta t)$ is the quantum Fisher information, i.e., the maximum of the Fisher information over all possible measurement schemes employing the photonic state in Eq. (1) [29,30].

The first inequality in Eq. (4) can always be saturated in the asymptotic regime of large N by the maximum-likelihood estimator [13,14] (see Appendix D), so we focus on the analysis of $F(\Delta t)$. The maximum precision achievable with the probe state in Eq. (1), given by the quantum Fisher information (see Appendix A)

$$H(\Delta t) = 2\sigma^2 = \frac{1}{2\tau^2} \equiv H, \quad (5)$$

is independent of the value of Δt to be estimated, with σ^2 the squared spectral bandwidth of each photon frequency probability distribution, i.e., the variance of $\bar{\xi}(\omega)^2$, and $\tau = 1/2\sigma$ the temporal bandwidth. Compared with the quantum Fisher information in the case of entangled photons generated with spontaneous parametric down-conversion with spectral bandwidth σ , the one in Eq. (5) is halved [10,15,31]. This means that, by only relying on independent photons, it is possible to achieve an ultimate precision that differs only by a constant factor $1/\sqrt{2}$ from the one achievable with entangled photons.

III. FISHER INFORMATION BASED ON FREQUENCY-RESOLVED MEASUREMENTS

We now determine the expression of the Fisher information for frequency-resolved measurements in the setup in Fig. 1. This includes the contribution from all the possible frequency-resolved events of photon bunching and coincidences occurring with the probabilities in Eq. (3), respectively. The Fisher information for such a scheme becomes (see Appendix C 1)

$$F_\eta(\Delta t) = \eta^4 \gamma^2 \mathcal{I}_\eta(\Delta t), \quad (6)$$

with

$$\begin{aligned} \mathcal{I}_\eta(\Delta t) &= \int_{\mathbb{R}^2} d\omega d\omega' \bar{\xi}(\omega)^2 \bar{\xi}(\omega')^2 (\omega - \omega')^2 \\ &\times \zeta_\eta[(\omega - \omega')\Delta t], \end{aligned} \quad (7)$$

where

$$\zeta_\eta(x) = \frac{\sin^2 x}{1 - \eta^4 \cos^2 x} \quad (8)$$

is for $\eta \neq 1$, a periodic function of period π oscillating between 0 and 1, whilst for $\eta = 1$, it becomes identically equal to 1.

We consider first the case where the photons differ only in the time they impinge on the beam splitter ($\eta = 1$). Because of the photon indistinguishability at the detectors arising from the frequency-resolved measurement, the Fisher information $F_{\eta=1}(\Delta t) \equiv F_{\eta=1}$ becomes independent of Δt and proportional to the quantum Fisher information in Eq. (5), i.e.,

$$F_{\eta=1} = \gamma^2 H = 2\gamma^2 \sigma^2 = \frac{\gamma^2}{2\tau^2}, \quad (9)$$

implying that shorter photons yield a more precise estimation. Remarkably, the detector efficiency only affects the estimation precision through a constant factor γ^2 , and, for lossless detectors $\gamma = 1$, the Fisher information equals the quantum Fisher information H found in Eq. (5). Therefore, this estimation scheme based on frequency-resolving measurements is optimal, and the level of high precision achieved is independent of the value of the delay to be estimated. Furthermore, $F_{\eta=1}$, similarly to H , is independent of the structure of the photonic wave packets, and it increases with the spectral variance σ^2 , for any value of the time delay Δt . In practical terms, if we assume a biphoton rate of 1 MHz and lossless detectors, employing photons with a temporal bandwidth of $\tau \sim 60$ fs within the reach of the state of the art [32,33], our frequency-resolving technique allows us to reach the attosecond precision in the estimation of any delay in only 2 h of measurements, while reducing τ to 10 fs would allow us to achieve the

same sensitivity in less than 4 min. In addition to high-precision measurements, our technique also allows for faster estimations.

We consider now the case $\eta < 1$ where the photons manifest some distinguishability at the detectors in parameters other than time. Of particular interest is the regime of small values of $\tau/\Delta t$. Indeed, when shorter and shorter temporal bandwidths τ , even smaller than Δt , are employed, the quantum Fisher information in Eq. (5) yields higher and higher sensitivities. The value of the Fisher information in Eq. (6) in such a regime, for regular photonic spectra (see Appendix C 2)

$$F_\eta(\tau/\Delta t \ll 1) = (1 - \sqrt{1 - \eta^4}) F_{\eta=1} \propto \frac{1}{\tau^2}, \quad (10)$$

is, for any value of $\eta < 1$, independent of Δt , proportional to the spectral variance σ^2 and independent of any other parameter in the wave packet distribution, as the quantum Fisher information H in Eq. (5).

The Cramér-Rao bound in Eq. (4) associated with the Fisher information in Eqs. (9) and (10) entails, for any value of η , an increase of precision when broader spectral bandwidths σ (shorter temporal bandwidths τ) are employed. This also overcomes the need for optimizing the reference path of the interferometer with high precision of the order of τ to maximize the Fisher information, as customary for nonresolved two-photon interference [9].

IV. EXAMPLE OF GAUSSIAN WAVE PACKETS

A typical experimental example is the case of Gaussian wave packets for which the Fisher information in Eq. (6) reduces to (see Appendix C 3)

$$F_\eta^G(\Delta t) = F_{\eta=1} \mathcal{I}_\eta^G \left(\frac{\Delta t}{\tau} \right), \quad (11)$$

with the integral

$$\mathcal{I}_\eta^G \left(\frac{\Delta t}{\tau} \right) = 2\eta^4 \sqrt{\frac{1}{\pi}} \int_{-\infty}^{\infty} d\kappa e^{-\kappa^2} \kappa^2 \zeta_\eta \left(\kappa \frac{\Delta t}{\tau} \right) \quad (12)$$

dependent on the periodic function ζ_η in Eq. (8).

As a practical comparison, the Fisher information in Eq. (11) manifests a clear metrological advantage with respect to the Fisher information associated with nonresolved (NR) two-photon interference measurements (see Appendix C 4)

$$F_\eta^{G,NR}(\Delta t) = F_{\eta=1} \frac{1}{2} \frac{\eta^4}{\exp[\frac{\Delta t^2}{2\tau^2}] - \eta^4} \frac{\Delta t^2}{\tau^2}. \quad (13)$$

In fact, as evident from Fig. 2, $F_\eta^G(\Delta t) > F_\eta^{G,NR}(\Delta t)$ independently of the indistinguishability η at the detectors,

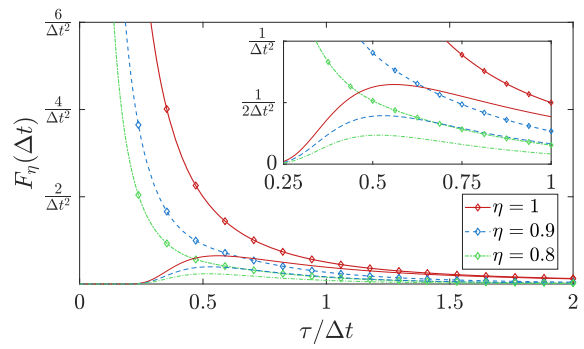


FIG. 2. Plots of the Fisher information $F_\eta(\Delta t) = F_\eta^G(\Delta t)$ for Gaussian photons in Eq. (11) (lines with markers) and $F_\eta(\Delta t) = F_\eta^{G,NR}(\Delta t)$ in Eq. (13) (thinner lines) as functions of the ratio $\tau/\Delta t$ between the photonic temporal bandwidth and the delay to be estimated. The nonresolving Fisher information quickly decreases for temporal bandwidths smaller than the optimal value $\tau \simeq \Delta t/2$, while the frequency-resolving Fisher information rapidly increases [see Eq. (10)]. This means that, for any given value of the delay, the quantum metrological advantage of resolved measurements increases in principle arbitrarily when employing shorter and shorter photons.

of the photonic spectral bandwidth σ , and of the value Δt to be estimated, leading to a quantum advantage of frequency-resolved measurements. In particular, for any given value of the delay Δt , when shorter and shorter photons are employed to maximize the quantum Fisher information, such quantum advantage $F^G(\Delta t)/F^{G,NR}(\Delta t)$ increases exponentially with $1/\tau$ (see Appendix C 3). Indeed, in the absence of information about the frequencies of the detected photons in the nonresolved technique, the estimation has to be restricted only to feasible experimental scenarios $\Delta t \simeq 2\tau$ (see Fig. 2), and it is not possible to take full advantage of the quadratic scaling with $1/\tau$ of the quantum Fisher information.

As a further advantage of the frequency-resolving technique, from the results obtained with numerical simulations shown in Fig. 3, it appears that the saturation of the Cramér-Rao bound in Eq. (4) when employing the maximum-likelihood estimator [13,14] is consistently achieved with less than 1000 observed samples independently of the value of the delay, differently from the nonresolving approach (see Appendix D). Moreover, the outcome of the frequency-resolving estimation appears to always yield finite estimates of Δt . Instead, in the nonresolving approach, the observed number of bunching and coincidence events can fail to provide a real and finite estimate of Δt due to statistical fluctuations. The corresponding fail probability drastically increases for larger delays, even if still of the order of τ , and for smaller values of the distinguishability η , even when we restrict ourselves to optimal values of the delay (see Appendix D).

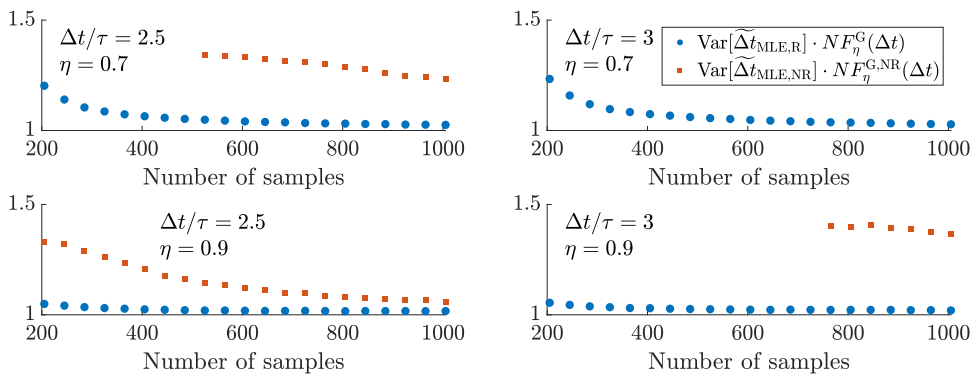


FIG. 3. Four numerical simulations have been carried out to test the rate of convergence of the variance of the maximum-likelihood estimator to the correspondent Cramér-Rao bound in Eq. (4) for the resolving (blue circles) and nonresolving (orange squares) technique for Gaussian spectra. Each point represents an average over 10^6 attempted iterations of the estimation. For the nonresolved approach, points where more than 1% of the estimations fail to yield a finite estimate are omitted (see Appendix D). Our technique appears to saturate the Cramér-Rao bound with fewer samples than in the nonresolving approach, particularly for decreasing values of $\tau/\Delta t$ and decreasing η .

V. CONCLUSIONS

We demonstrate the quantum metrological advantage in the estimation of the time delay between two photons with the same frequency distribution in a two-photon interference setup with frequency-resolving detectors. We show that, for photons with arbitrary time delay, sampling from the coincidence and bunching probabilities, and additionally from all the possible photonic frequencies, is an optimal estimation strategy—in the sense that it saturates the ultimate precision given by the quantum Cramér-Rao bound.

Even for pairs of photons with any degree of nontemporal distinguishability in the measurement (e.g., polarization), this frequency-resolved technique still outperforms nonresolving measurements, for any value of the spectral bandwidth and of the time delay to be estimated. This enhancement in precision is especially significant with ultrashort photons, even shorter than the time delay to be estimated, since both the quantum Fisher information and the frequency-resolving Fisher information increase quadratically with the photonic spectral bandwidth. Indeed, independently of the value of the time delay to estimate, there is no upper limit, in principle, to the maximum achievable precision, particularly in view of future sources able to generate shorter and shorter photons. This is not the case for nonresolved interferometers, where the maximum precision (achievable only after a prior optimization of the setup) is fundamentally limited in value for any fixed delay, and the sensitivity decreases exponentially with smaller and smaller overlap between the photonic wave packets [9]. Moreover, it appears that, compared with the nonresolving technique, fewer samples are required to saturate the Cramér-Rao bound through the maximum-likelihood estimator.

Furthermore, the precision of this technique is not limited by the detector time resolution required to resolve directly the time delay as in time-resolved measurements [15]. Indeed, this constraint is circumvented by a much less demanding resolution in the frequency domain that aims only to ensure photon indistinguishability in time at the detectors independently of the precision one wants to achieve in the estimation. Instead, such a precision is fundamentally limited mainly by the minimum achievable temporal bandwidth of the photons. These results have therefore the potential to substantially improve the precision and the duration of the measurement of current and future sensing techniques (e.g., optical coherence tomography [34], quantitative phase microscopy [35], holographic interference microscopy [36]) employing photons that are shorter than the delay to be measured, with applications, among others, in biomedical sensing [37,38], such as surface roughness characterization [39], and more in general in the characterization of any semitransparent sample.

From a more fundamental perspective, the proposed technique unravels the full metrological power of frequency-resolved sampling measurements allowing us to infer high-precision information about the photon in the conjugate (time) domain that would otherwise be completely lost. We also emphasize that it is possible to operate the same technique to enhance the precision of two-photon interference protocols for the estimation of the frequency shift between two independent photons through time-resolving measurements, i.e., inverting the role of the two conjugate variables. These results are thus applicable, in principle, to general estimation schemes based on any pair of conjugate parameters, such as position and momentum or angular position and orbital angular momentum. They also lay the foundations for future schemes based on multiparameter resolved measurements able to

increase the indistinguishability of photons at the detectors in multiple degrees of freedom, and therefore, enhance the metrological capabilities of multiphoton interference techniques.

Finally, an extension of such results to more than two photons could lead in future works to the demonstration of a quantum metrological advantage of inner-mode variables multiphoton interference in more general linear optical networks with a larger number N of nonentangled input photons based on sampling in suitable photonic inner degrees of freedom at the interferometer output [24]. The extension of this technique to an optical network with two or more entangled photons will be also addressed in future works.

ACKNOWLEDGMENTS

We thank Paolo Facchi and Frank A. Narducci for the helpful discussions. This work is partially supported by the Office of Naval Research Global (N62909-18-1-2153).

APPENDIX A: QUANTUM FISHER INFORMATION

In this section we evaluate the quantum Fisher information in Eq. (5) in the main text. To do so, we first need to rewrite the probe state $|\psi\rangle$ in Eq. (1) in terms of the delay Δt between the two photons. In the following treatment, we suppose that all the moments of the frequency distribution of the two photons are known, as well as the distinguishability parameter η , while the time delay $\Delta t = t_1 - t_2$ and the sum of the emission times $t_{\text{tot}} = t_1 + t_2$ are unknown, as is customary in experimental scenarios. Since in this setup two unknown parameter are present, the formal approach to this estimation problem requires the employment of the 2×2 quantum Fisher information matrix (QFIM) \mathcal{H} [29,30,40], whose elements are given by

$$\mathcal{H}_{ij} = 4\text{Re}[\langle \partial_i \psi | \partial_j \psi \rangle - \langle \psi | \partial_i \psi \rangle^* \langle \psi | \partial_j \psi \rangle], \quad i, j = 1, 2, \quad (\text{A1})$$

where we denote with $\partial_1 \equiv \partial_-$ and $\partial_2 \equiv \partial_+$ the derivatives with respect to Δt and t_{tot} , respectively, while the quantum Cramér-Rao bound is given in matrix form as

$$\text{Cov}[\{\Delta t, t_{\text{tot}}\}] \geq \frac{\mathcal{H}^{-1}}{N}. \quad (\text{A2})$$

We show that the QFIM is diagonal, so that the Cramér-Rao bound associated with the time delay can be written only in terms of $\mathcal{H}_{11} \equiv H(\Delta t)$, with $H(\Delta t)$ shown in Eq. (5).

First, we rewrite the state $|\psi\rangle$ from Eq. (1),

$$\begin{aligned} |\psi\rangle &= \int_{\mathbb{R}^2} d\omega_1 d\omega_2 \bar{\xi}(\omega_1) \bar{\xi}(\omega_2) e^{-i\omega_1 t_1 - i\omega_2 t_2} \\ &\quad \times (\eta \hat{a}_{1,\omega_1}^\dagger + \sqrt{1 - \eta^2} \hat{b}_{1,\omega_1}^\dagger) \hat{a}_{2,\omega_2}^\dagger |\text{vac}\rangle, \\ &= \int_{\mathbb{R}^2} d\omega_1 d\omega_2 \bar{\xi}(\omega_1) \bar{\xi}(\omega_2) e^{-it_{\text{tot}}(\omega_1 + \omega_2)/2 - i\Delta t(\omega_1 - \omega_2)/2} \\ &\quad \times (\eta \hat{a}_{1,\omega_1}^\dagger + \sqrt{1 - \eta^2} \hat{b}_{1,\omega_1}^\dagger) \hat{a}_{2,\omega_2}^\dagger |\text{vac}\rangle. \end{aligned} \quad (\text{A3})$$

It is straightforward to evaluate the derivatives $|\partial_1 \psi\rangle \equiv |\partial_- \psi\rangle$ and $|\partial_2 \psi\rangle \equiv |\partial_+ \psi\rangle$ as

$$\begin{aligned} |\partial_\pm \psi\rangle &= \frac{1}{2i} \int_{\mathbb{R}^2} d\omega_1 d\omega_2 e^{-it_{\text{tot}} \frac{\omega_1 + \omega_2}{2} - i\Delta t \frac{\omega_1 - \omega_2}{2}} (\omega_1 \pm \omega_2) \\ &\quad \times \bar{\xi}(\omega_1) \bar{\xi}(\omega_2) (\eta \hat{a}_{1,\omega_1}^\dagger + \sqrt{1 - \eta^2} \hat{b}_{1,\omega_1}^\dagger) \hat{a}_{2,\omega_2}^\dagger |\text{vac}\rangle. \end{aligned} \quad (\text{A4})$$

To evaluate the scalar products in Eq. (A1), it is useful to first note that

$$\begin{aligned} \langle \text{vac} | (\eta \hat{a}_{1,\omega_3} + \sqrt{1 - \eta^2} \hat{b}_{1,\omega_3}) (\eta \hat{a}_{1,\omega_1}^\dagger + \sqrt{1 - \eta^2} \hat{b}_{1,\omega_1}^\dagger) \\ \times \hat{a}_{2,\omega_4} \hat{a}_{2,\omega_2}^\dagger | \text{vac} \rangle = \delta(\omega_1 - \omega_3) \delta(\omega_2 - \omega_4), \end{aligned} \quad (\text{A5})$$

where $\delta(\cdot)$ is the Dirac delta distribution. Now we can easily evaluate the scalar products

$$\begin{aligned} \langle \partial_- \psi | \partial_- \psi \rangle &= \frac{1}{4} \int_{\mathbb{R}^2} d\omega_1 d\omega_2 (\omega_1 - \omega_2)^2 \bar{\xi}(\omega_1)^2 \bar{\xi}(\omega_2)^2 \\ &= \frac{1}{2} \sigma^2 \\ \langle \partial_+ \psi | \partial_+ \psi \rangle &= \frac{1}{4} \int_{\mathbb{R}^2} d\omega_1 d\omega_2 (\omega_1 + \omega_2)^2 \bar{\xi}(\omega_1)^2 \bar{\xi}(\omega_2)^2 \\ &= \frac{1}{2} (\sigma^2 + 2\omega_0^2) \\ \langle \partial_- \psi | \partial_+ \psi \rangle &= \frac{1}{4} \int_{\mathbb{R}^2} d\omega_1 d\omega_2 (\omega_1^2 - \omega_2^2) \bar{\xi}(\omega_1)^2 \bar{\xi}(\omega_2)^2 = 0 \\ \langle \psi | \partial_- \psi \rangle &= \frac{1}{2i} \int_{\mathbb{R}^2} d\omega_1 d\omega_2 (\omega_1 - \omega_2) \bar{\xi}(\omega_1)^2 \bar{\xi}(\omega_2)^2 = 0 \\ \langle \psi | \partial_+ \psi \rangle &= \frac{1}{2i} \int_{\mathbb{R}^2} d\omega_1 d\omega_2 (\omega_1 + \omega_2) \bar{\xi}(\omega_1)^2 \bar{\xi}(\omega_2)^2 \\ &= -i\omega_0, \end{aligned} \quad (\text{A6})$$

where ω_0 and σ^2 are the central frequency and variance of the frequency distribution $\bar{\xi}(\omega)^2$, and finally, by substituting Eq. (A6) into Eq. (A1), we obtain the QFIM

$$\mathcal{H} = \begin{pmatrix} 2\sigma^2 & 0 \\ 0 & 2\sigma^2 \end{pmatrix}, \quad (\text{A7})$$

which is diagonal, and the element $H(\Delta t)$ associated with the delay Δt is the value in Eq. (5) appearing in the quantum Cramér-Rao bound shown in Eq. (4) in the main text.

APPENDIX B: BUNCHING AND COINCIDENCE PROBABILITIES

Here, we evaluate the probability in Eq. (3) that the two photons are observed with frequencies ω_1, ω_2 in the same and in different output channels.

The balanced beam splitter, on which the two photons in the state $|\psi\rangle$ in Eq. (1) impinge, can be described with a 2×2 unitary matrix U_{BS} of transition amplitudes

$$U_{\text{BS}} = \frac{1}{\sqrt{2}} \begin{pmatrix} 1 & -1 \\ 1 & 1 \end{pmatrix}, \quad (\text{B1})$$

and it acts on the injected probe through the map $\hat{U}_{\text{BS}} \hat{a}_i^\dagger \hat{U}_{\text{BS}}^\dagger = \sum_{j=1,2} (U_{\text{BS}})_{ij} \hat{a}_j^\dagger$, and equivalently for \hat{b}_i^\dagger . With reference to Eq. (1), the two-photon state $|\psi'\rangle$ at the output of the beam splitter thus reads

$$\begin{aligned} |\psi'\rangle &= \hat{U}_{\text{BS}} |\psi\rangle = \frac{1}{2} \int_{\mathbb{R}^2} d\omega_1 d\omega_2 \xi_1(\omega_1) \xi_2(\omega_2) [\eta (\hat{a}_{1,\omega_1}^\dagger - \hat{a}_{2,\omega_1}^\dagger) + \sqrt{1-\eta^2} (\hat{b}_{1,\omega_1}^\dagger - \hat{b}_{2,\omega_1}^\dagger)] (\hat{a}_{1,\omega_2}^\dagger + \hat{a}_{2,\omega_2}^\dagger) |\text{vac}\rangle \\ &= \frac{1}{2} \int_{\mathbb{R}^2} d\omega_1 d\omega_2 \xi_1(\omega_1) \xi_2(\omega_2) [\eta (\hat{a}_{1,\omega_1}^\dagger \hat{a}_{1,\omega_2}^\dagger - \hat{a}_{2,\omega_1}^\dagger \hat{a}_{2,\omega_2}^\dagger + \hat{a}_{1,\omega_1}^\dagger \hat{a}_{2,\omega_2}^\dagger - \hat{a}_{2,\omega_1}^\dagger \hat{a}_{1,\omega_2}^\dagger) \\ &\quad + \sqrt{1-\eta^2} (\hat{b}_{1,\omega_1}^\dagger \hat{a}_{1,\omega_2}^\dagger - \hat{b}_{2,\omega_1}^\dagger \hat{a}_{2,\omega_2}^\dagger + \hat{b}_{1,\omega_1}^\dagger \hat{a}_{2,\omega_2}^\dagger - \hat{b}_{2,\omega_1}^\dagger \hat{a}_{1,\omega_2}^\dagger)]. \end{aligned} \quad (\text{B2})$$

In order to evaluate the probabilities that two photons with frequencies ω and ω' are observed in each configuration (bunching or coincidence), it is convenient to further manipulate Eq. (B2) to more easily take into account the indistinguishability of identical photons, so that

$$\begin{aligned} |\psi'\rangle &= \frac{\eta}{2} \int_{\omega_1 < \omega_2} d\omega_1 d\omega_2 [\xi_1(\omega_1) \xi_2(\omega_2) + \xi_1(\omega_2) \xi_2(\omega_1)] [\hat{a}_{1,\omega_1}^\dagger \hat{a}_{1,\omega_2}^\dagger - \hat{a}_{2,\omega_1}^\dagger \hat{a}_{2,\omega_2}^\dagger] |\text{vac}\rangle \\ &\quad + \frac{\eta}{2} \int_{\omega_1 < \omega_2} d\omega_1 d\omega_2 [\xi_1(\omega_1) \xi_2(\omega_2) - \xi_1(\omega_2) \xi_2(\omega_1)] [\hat{a}_{1,\omega_1}^\dagger \hat{a}_{2,\omega_2}^\dagger - \hat{a}_{2,\omega_1}^\dagger \hat{a}_{1,\omega_2}^\dagger] |\text{vac}\rangle \\ &\quad + \frac{\sqrt{1-\eta^2}}{2} \int_{\mathbb{R}^2} d\omega_1 d\omega_2 \xi_1(\omega_1) \xi_2(\omega_2) (\hat{b}_{1,\omega_1}^\dagger \hat{a}_{1,\omega_2}^\dagger - \hat{b}_{2,\omega_1}^\dagger \hat{a}_{2,\omega_2}^\dagger + \hat{b}_{1,\omega_1}^\dagger \hat{a}_{2,\omega_2}^\dagger - \hat{b}_{2,\omega_1}^\dagger \hat{a}_{1,\omega_2}^\dagger) |\text{vac}\rangle, \end{aligned} \quad (\text{B3})$$

can be written as a sum of three contributes: the first associated with photons ending up in the same channel and in the mode described by the operator $\hat{a}_{i,\omega_j}^\dagger$, the second with the photons ending up in different channels in the mode described by the operator $\hat{a}_{i,\omega_j}^\dagger$, and the third is the contribution given when the distinguishability in the inner properties other than time and frequency (e.g., polarization) is observed at the detectors. Hence, the probability $p_B([\omega - \delta\omega/2, \omega + \delta\omega/2], [\omega' - \delta\omega/2, \omega' + \delta\omega/2])$ to observe the two photons together in any of the output channels with frequencies ω, ω' within the resolution $\delta\omega$ is given by

$$\begin{aligned} p_B([\omega - \delta\omega/2, \omega + \delta\omega/2], [\omega' - \delta\omega/2, \omega' + \delta\omega/2]) &= \int_{\omega-\delta\omega/2}^{\omega+\delta\omega/2} \int_{\omega'-\delta\omega/2}^{\omega'+\delta\omega/2} dw_1 dw_2 \sum_{i=1,2} |\langle \text{vac} | \hat{a}_{i,w_1} \hat{a}_{i,w_2} | \psi' \rangle|^2 + |\langle \text{vac} | \hat{a}_{i,w_1} \hat{b}_{i,w_2} | \psi' \rangle|^2 + |\langle \text{vac} | \hat{b}_{i,w_1} \hat{a}_{i,w_2} | \psi' \rangle|^2 \\ &= \int_{\omega-\delta\omega/2}^{\omega+\delta\omega/2} \int_{\omega'-\delta\omega/2}^{\omega'+\delta\omega/2} dw_1 dw_2 \left\{ \frac{\eta^2}{2} |\xi_1(w_1) \xi_2(w_2) + \xi_1(w_2) \xi_2(w_1)|^2 + \frac{1-\eta^2}{2} [|\xi_1(w_1) \xi_2(w_2)|^2 + |\xi_1(w_2) \xi_2(w_1)|^2] \right\} \\ &= \frac{1}{2} \{ |\xi_1(\omega) \xi_2(\omega')|^2 + |\xi_1(\omega') \xi_2(\omega)|^2 + 2\eta^2 \operatorname{Re}[\xi_1(\omega) \xi_2(\omega') \xi_1^*(\omega') \xi_2^*(\omega)] \} \delta\omega \delta\omega' \equiv p_B(\omega, \omega') \delta\omega^2, \end{aligned} \quad (\text{B4})$$

where, in the last step, we assume that the resolution $\delta\omega$ is small enough so that the variations of the integrand are negligible, which is guaranteed if the conditions in Eq. (2) are verified. Similar considerations can be done for the probability of coincidence $p_C([\omega - \delta\omega/2, \omega + \delta\omega/2], [\omega' - \delta\omega/2, \omega' + \delta\omega/2])$ for photons ending up in different channels,

$$\begin{aligned}
& p_C([\omega - \delta\omega/2, \omega + \delta\omega/2], [\omega' - \delta\omega/2, \omega' + \delta\omega/2]) \\
&= \int_{\omega-\delta\omega/2}^{\omega+\delta\omega/2} \int_{\omega'-\delta\omega/2}^{\omega'+\delta\omega/2} dw_1 dw_2 (|\langle \text{vac} | \hat{a}_{1,w_1} \hat{a}_{2,w_2} | \psi' \rangle|^2 + |\langle \text{vac} | \hat{a}_{1,w_1} \hat{b}_{2,w_2} | \psi' \rangle|^2 + |\langle \text{vac} | \hat{b}_{1,w_1} \hat{a}_{2,w_2} | \psi' \rangle|^2 \\
&\quad + |\langle \text{vac} | \hat{a}_{1,w_2} \hat{a}_{2,w_1} | \psi' \rangle|^2 + |\langle \text{vac} | \hat{a}_{1,w_2} \hat{b}_{2,w_1} | \psi' \rangle|^2 + |\langle \text{vac} | \hat{b}_{1,w_2} \hat{a}_{2,w_1} | \psi' \rangle|^2) \\
&= \int_{\omega-\delta\omega/2}^{\omega+\delta\omega/2} \int_{\omega'-\frac{\delta\omega}{2}}^{\omega'+\frac{\delta\omega}{2}} dw_1 dw_2 \left\{ \frac{\eta^2}{2} |\xi_1(w_1)\xi_2(w_2) - \xi_1(w_2)\xi_2(w_1)|^2 + \frac{1-\eta^2}{2} [|\xi_1(w_1)\xi_2(w_2)|^2 + |\xi_1(w_2)\xi_2(w_1)|^2] \right\} \\
&= \frac{1}{2} \{ |\xi_1(\omega)\xi_2(\omega')|^2 + |\xi_1(\omega')\xi_2(\omega)|^2 - 2\eta^2 \text{Re}[\xi_1(\omega)\xi_2(\omega')\xi_1^*(\omega')\xi_2^*(\omega)] \} \delta\omega \delta\omega' \equiv p_C(\omega, \omega') \delta\omega^2. \tag{B5}
\end{aligned}$$

Let us now suppose that the frequency distributions are of the form $\xi_i(\omega) = \bar{\xi}(\omega) e^{-i\omega t_i}$, with $\bar{\xi}(\omega)$ real and independent on t_i , for $i = 1, 2$, so that, following from Eqs. (B4) and (B5),

$$\begin{aligned}
p_B(\omega, \omega') &= \bar{\xi}(\omega)^2 \bar{\xi}(\omega')^2 \{1 + \eta^2 \cos[(\omega - \omega')\Delta t]\}, \\
p_C(\omega, \omega') &= \bar{\xi}(\omega)^2 \bar{\xi}(\omega')^2 \{1 - \eta^2 \cos[(\omega - \omega')\Delta t]\}. \tag{B6}
\end{aligned}$$

In the case of imperfect detectors detecting a single incoming photon with probability γ^2 , the probability distributions associated with the events of two-photon bunching and two-photon coincidences at the detectors are, respectively,

$$\begin{aligned}
P_\eta^B(\omega, \omega') &= \gamma^2 p_B(\omega, \omega') \\
&= \gamma^2 \bar{\xi}(\omega)^2 \bar{\xi}(\omega')^2 \{1 + \eta^2 \cos[(\omega - \omega')\Delta t]\} \\
P_\eta^C(\omega, \omega') &= \gamma^2 p_C(\omega, \omega') \\
&= \gamma^2 \bar{\xi}(\omega)^2 \bar{\xi}(\omega')^2 \{1 - \eta^2 \cos[(\omega - \omega')\Delta t]\}. \tag{B7}
\end{aligned}$$

from which we find the expression in Eq. (3). On the other hand, as one may expect, the probabilities

$$\begin{aligned}
P_0 &= \gamma^2 \\
P_1(\omega) &= \gamma(1-\gamma) \left\{ \int_{\mathbb{R}} d\omega' [p_\eta^B(\omega, \omega') + p_\eta^C(\omega, \omega')] \right\} \\
&= 2\gamma(1-\gamma) \bar{\xi}(\omega)^2 \tag{B8}
\end{aligned}$$

of detecting no photons or only a single photon, respectively, do not yield any information on Δt , and thus, do not contribute to the Fisher information.

APPENDIX C: FISHER INFORMATION

1. Arbitrary frequency spectra

In order to evaluate the Fisher information in Eq. (6) associated with the estimation of Δt , we evaluate from the relevant expressions of the probabilities of bunching and coincidence in Eq. (B7),

$$\begin{aligned}
\frac{d}{d\Delta t} P_\eta^B(\omega, \omega') &= -\frac{d}{d\Delta t} P_\eta^C(\omega, \omega') \\
&= -\gamma^2 \bar{\xi}(\omega)^2 \bar{\xi}(\omega')^2 \eta^2 (\omega - \omega') \sin[(\omega - \omega')\Delta t], \tag{C1}
\end{aligned}$$

and thus, from the definition of Fisher information

$$F(\Delta t) = \mathbb{E} \left\{ \left[\frac{d}{d\Delta t} \log p(X | \Delta t) \right]^2 \right\}, \tag{C2}$$

with X denoting the random outcome of the measurement procedure (i.e., frequencies detected and bunching or coincidence detection), we obtain

$$\begin{aligned}
F_\eta(\Delta t) &= \int_{\omega < \omega'} d\omega d\omega' \left\{ \frac{1}{P_\eta^B(\omega, \omega')} \left[\frac{d}{d\Delta t} P_\eta^B(\omega, \omega') \right]^2 \right. \\
&\quad \left. + \frac{1}{P_\eta^C(\omega, \omega')} \left[\frac{d}{d\Delta t} P_\eta^C(\omega, \omega') \right]^2 \right\} \\
&= \eta^4 \gamma^2 \int_{\mathbb{R}^2} d\omega d\omega' \bar{\xi}(\omega)^2 \bar{\xi}(\omega')^2 (\omega - \omega')^2 \\
&\quad \times \frac{\sin^2[(\omega - \omega')\Delta t]}{1 - \eta^4 \cos^2[(\omega - \omega')\Delta t]} = \eta^4 \gamma^2 \mathcal{I}_\eta(\Delta t), \tag{C3}
\end{aligned}$$

which corresponds to Eq. (6).

2. Regime $\Delta t \gg \tau$

We analyze now the Fisher information $F_\eta(\Delta t)$ in the regime of large time delays $\Delta t \gg \tau$, obtaining the expression in Eq. (10). We first note that the function $\zeta_\eta[(\omega - \omega')\Delta t]$ in Eq. (8) oscillates in $\omega - \omega'$, with period $\pi/\Delta t$. If the frequency spectrum $\bar{\xi}(\omega)^2$ of the two photons is regular enough (as for Gaussian wave packets) so that it does not present intrinsic fast fluctuations, we can assume that the rest of the integrand in the Fisher information in Eq. (6) is essentially constant within the periodicity interval $\pi/\Delta t$ much smaller than the photonic bandwidth $\sigma = 1/(2\tau)$ in the regime $\Delta t \gg \tau$. It is then possible to substitute $\zeta_\eta[(\omega - \omega')\Delta t]$ with its average over its period in Eq. (6), which reads

$$\frac{\Delta t}{\pi} \int_{[0,\pi/\Delta t]} d\omega \zeta_\eta(\omega\Delta t) = \frac{1 - \sqrt{1 - \eta^4}}{\eta^4}. \quad (\text{C4})$$

Replacing $\zeta_\eta[(\omega - \omega')\Delta t]$ in Eq. (6) with the right-hand term in Eq. (C4), we obtain

$$\begin{aligned} F_\eta(\Delta t \gg \tau) &= 2(1 - \sqrt{1 - \eta^4})\gamma^2\sigma^2 \\ &= (1 - \sqrt{1 - \eta^4})F_{\eta=1}, \end{aligned} \quad (\text{C5})$$

as shown in Eq. (10).

3. Gaussian spectra

Now we obtain the specialized expressions for the Fisher information $\mathcal{F}_\eta^G(\Delta t)$ shown in Eq. (11) associated with Gaussian photons, with spectra

$$\bar{\xi}(\omega)^2 = \sqrt{\frac{1}{2\pi\sigma^2}} \exp\left[-\frac{(\omega - \Omega_0)^2}{2\sigma^2}\right], \quad (\text{C6})$$

where Ω_0 is the central frequency and σ^2 is the variance. By substituting Eq. (C6) into Eq. (C3), we obtain

$$\begin{aligned} F_\eta(\Delta t) &= \eta^4\gamma^2 \frac{1}{2\pi\sigma^2} \int d\omega d\omega' e^{-(1/2\sigma^2)[(\omega - \Omega_0)^2 + (\omega' - \Omega_0)^2]} \\ &\times (\omega - \omega')^2 \zeta[(\omega - \omega')\Delta t]. \end{aligned} \quad (\text{C7})$$

With a change of variables $\delta = \omega - \omega'$, $s = \omega + \omega' - 2\Omega_0$, we get

$$\begin{aligned} F_\eta(\Delta t) &= \eta^4\gamma^2 \frac{1}{4\pi\sigma^2} \int d\delta ds e^{-(s^2 + \delta^2)/(4\sigma^2)} \delta^2 \zeta(\delta\Delta t) \\ &= \eta^4\gamma^2 \sqrt{\frac{1}{4\pi\sigma^2}} \int d\delta e^{-(\delta^2)/(4\sigma^2)} \delta^2 \zeta(\delta\Delta t), \\ &= \eta^4\gamma^2 \sqrt{\frac{\tau^2}{\pi}} \int d\delta e^{-\tau^2\delta^2} \delta^2 \zeta(\delta\Delta t). \end{aligned} \quad (\text{C8})$$

A further change of variable to the dimensionless parameter $\kappa = \delta\tau$, finally yields

$$F_\eta(\Delta t) = \frac{\eta^4\gamma^2}{\tau^2} \sqrt{\frac{1}{\pi}} \int d\kappa e^{-\kappa^2} \kappa^2 \zeta\left(\kappa \frac{\Delta t}{\tau}\right) \quad (\text{C9})$$

corresponding to the expression for the Fisher information $F_\eta^G(\Delta t)$ in Eq. (11). From Eq. (C9), we can easily obtain the dimensionless quantities

$$F_\eta(\Delta t)\Delta t^2 = \frac{\Delta t^2}{\tau^2} \eta^4\gamma^2 \sqrt{\frac{1}{\pi}} \int d\kappa e^{-\kappa^2} \kappa^2 \zeta\left(\kappa \frac{\Delta t}{\tau}\right), \quad (\text{C10a})$$

$$F_\eta(\Delta t)\tau^2 = \eta^4\gamma^2 \sqrt{\frac{1}{\pi}} \int d\kappa e^{-\kappa^2} \kappa^2 \zeta\left(\kappa \frac{\Delta t}{\tau}\right), \quad (\text{C10b})$$

which only depend on the dimensionless parameters $\Delta t/\tau$, η , and γ .

4. Comparison with nonresolving approach

We now obtain the expression of the Fisher information in Eq. (13) for nonresolved measurements. If instead the frequencies of the two photons are not observed, the probabilities of bunching and coincidence events can be found by summing the probability in Eq. (3) over all the possible frequencies ω, ω' obtaining

$$P_\eta^B = \int_{\omega < \omega'} d\omega d\omega' P_\eta^B(\omega, \omega'), \quad (\text{C11a})$$

$$P_\eta^C = \int_{\omega < \omega'} d\omega d\omega' P_\eta^C(\omega, \omega'). \quad (\text{C11b})$$

Note how the effect of nonresolving the frequencies anticipates the integration over all the frequencies of the photons, which is here performed on the probabilities instead of while evaluating the expectation value of the Fisher information in Eq. (6).

If we assume that the photons are Gaussian, with spectra given in Eq. (C6), the probabilities in Eq. (C11) become

$$P_\eta^B = \frac{\gamma^2}{2}(1 + \eta^2 e^{-\Delta t^2\sigma^2}), \quad (\text{C12a})$$

$$P_\eta^C = \frac{\gamma^2}{2}(1 - \eta^2 e^{-\Delta t^2\sigma^2}). \quad (\text{C12b})$$

It is straightforward to see, by applying the definition in Eq. (C2), that the expression of the Fisher information

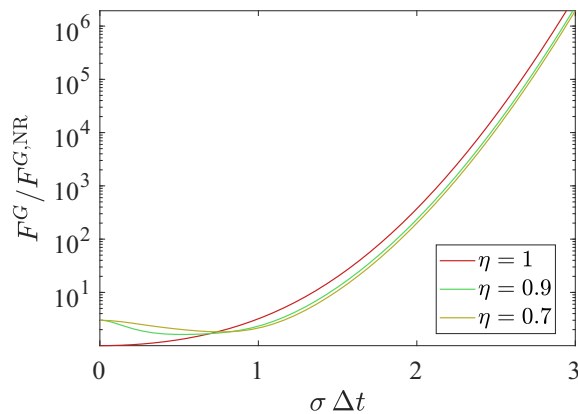


FIG. 4. Enhancement factor $F^G/F^{G,NR}$ achieved through frequency-resolving detectors with respect to nonresolving techniques, as a function of $\sigma \Delta t \equiv \Delta t/(2\tau)$ and for different values of η . We can see that, for a fixed delay between photons, the enhancement factor increases exponentially with the spectral width σ , taking values close to 2 for $\sigma \Delta t \simeq 1$, becoming approximately 10^2 for $\sigma \Delta t \simeq 2$, and 10^6 for $\sigma \Delta t \simeq 3$.

associated with nonresolving measurements is

$$\begin{aligned} F_\eta^{G,NR}(\Delta t) &= 4\gamma^2 \frac{\eta^4}{\exp[2\Delta t^2\sigma^2] - \eta^4} \Delta t^2 \sigma^4 \\ &\equiv \frac{1}{2} F_{\eta=1} \frac{\eta^4}{\exp[\frac{\Delta t^2}{2\tau^2}] - \eta^4} \frac{\Delta t^2}{\tau^2}, \end{aligned} \quad (\text{C13})$$

as in Eq. (13) with $F_{\eta=1} = 2\gamma^2\sigma^2 \equiv \gamma^2/(2\tau^2)$.

The advantage of the frequency-resolving technique, compared with nonresolving estimation schemes, is clearly visible in Fig. 4, where the exponential increase of the enhancement factor $F^G(\Delta t)/F^{G,NR}(\Delta t)$ between the frequency-resolving and non-resolving approaches for increasing values of $\sigma \Delta t$ is displayed. It is important to note that the enhancement factor also represent the ratio $N^{G,NR}/N^G$ of photon pairs required to reach a given precision with nonresolving and resolving detectors, for schemes saturating the Cramér-Rao bound in Eq. (4). In other words, an enhancement factor of 10^6 , achieved, for example, for $\sigma \Delta t = 3$, translates into a theoretical reduction of experimental events that need to be observed of a factor 10^6 , with a remarkable impact on the duration of the experiment.

APPENDIX D: NUMERICAL SIMULATION OF AN EFFICIENT ESTIMATOR

We dedicate this section to propose and to analyze an experimental strategy that practically achieves the Cramér-Rao bound in Eq. (4). In particular, this strategy employs the well-known maximum-likelihood estimator, which is renownedly asymptotically unbiased and efficient, i.e., it saturates the Cramér-Rao bound in the regime of large

samples [13,14]. We thus devote our numerical analysis to understand how populated the sample of experimental data must be in order to practically consider this ultimate bound saturated. We perform the numerical analysis for the case of Gaussian spectra discussed in the main text.

Let us imagine operating the frequency-resolving interferometer for a given period of time, in which we manage to observe $N_\gamma \equiv N\gamma^2$ two-photon events. In doing so, we are already taking into account that a portion $N(1 - \gamma^2)$ of events must be discarded since they do not yield any information on the time delay due to losses (only one or no photons are detected). In fact, we note from Eqs. (4) and (6) that the Cramér-Rao bound we evaluate is equivalent to the same bound in a lossless scenario, but with $N\gamma^2$ pairs of photons at our disposal. We thus consider from now on a setup without losses, but which employs only a fraction $N_\gamma \equiv N\gamma^2$ of photon pairs.

The outcome of the i th observed event $s^{(i)} = (\omega_1^{(i)}, \omega_2^{(i)}, X_i)$, with $i = 1, \dots, N_\gamma$ will contribute to the experimental sample $S_{N_\gamma} = \{s^{(i)}\}_{i=1, \dots, N_\gamma}$ with the joint information regarding the frequencies $\omega_1^{(i)}, \omega_2^{(i)}$ of the two photons, and whether they ended up in the same output channel of the beam splitter or not, i.e., $X_i = C$ for coincidence or $X_i = B$ for bunching photons. Assuming that the resolution $\delta\omega$ of the detectors satisfies conditions in Eq. (2), and that their working range practically spans over the whole photonic spectra, each outcome of the experiment will be exactly generated according to the probability distribution given by Eq. (3) with $\gamma = 1$, namely,

$$P(s^{(i)}, \Delta t) \delta\omega^2 = P_{\eta}^{X_i}(\omega_1^{(i)}, \omega_2^{(i)}) \delta\omega^2, \quad (\text{D1})$$

where we emphasized the dependency of this probability on the unknown delay Δt .

Since each repetition of the experiment is performed independently from the others, the probability $P(S_{N_\gamma})$ associated with the whole sample S_{N_γ} is given by the product

$$P(S_{N_\gamma}, \Delta t) \delta\omega^{2N_\gamma} = \prod_{i=1}^{N_\gamma} P(s^{(i)}, \Delta t) \delta\omega^2 \quad (\text{D2})$$

of the single event probabilities. The expression in Eq. (D2) can be thought of as a function $\mathcal{L}_R(\Delta t | S_{N_\gamma}) \equiv P(S_{N_\gamma}, \Delta t)$ of Δt , typically called likelihood function, yielding the probability (up to a factor $\delta\omega^{2N_\gamma}$) that the observed sample S_{N_γ} is randomly generated according to the value Δt of the delay. Noticeably, for every possible value Δt , the likelihood $\mathcal{L}_R(\Delta t | S_{N_\gamma})$ is a number that can be easily evaluated through Eq. (D2) once the data sample S_{N_γ} has been obtained.

The strategy we propose then makes use of the maximum-likelihood estimator $\tilde{\Delta t}_{MLE}$ to retrieve an estimate of the delay true unknown value, which is thus given

by the quantity that maximizes the likelihood function, i.e., it is implicitly defined by

$$\mathcal{L}_R(\tilde{\Delta}t_{MLE} | S_{N_\gamma}) = \sup_{\Delta t} \mathcal{L}_R(\Delta t | S_{N_\gamma}). \quad (D3)$$

The advantage of employing the maximum-likelihood estimator is that for large numbers of samples, i.e., large N_γ , it is asymptotically unbiased and efficient, in the sense that, in this regime, its expectation value equals the true value of the unknown delay Δt , and its variance saturates the Cramér-Rao Bound, i.e., $\mathbb{E}[\tilde{\Delta}t_{MLE}] = \Delta t$ and $\text{Var}[\tilde{\Delta}t_{MLE}] = [N\mathcal{F}_\eta(\Delta t)]^{-1}$. On the other hand, Eq. (D3) cannot be solved analytically in general, e.g., in the case of Gaussian spectra we examined previously, so a numerical approach is usually undertaken to maximize the likelihood function $\mathcal{L}_R(\Delta t | S_{N_\gamma})$.

Lastly, in Fig. 3 in the main text and in Figs. 5–7, we test unbiasedness and efficiency of the maximum-likelihood estimator for different numbers N_γ of the observed samples S_{N_γ} , comparing the results of our frequency-resolving strategy with a nonresolving one, for example, the time-delay estimation based on maximum likelihood in Ref. [9]. We see how both the unbiasedness and the efficiency of the maximum-likelihood estimator are reached for a

number $N_\gamma \leq 1000$ independently of Δt for the frequency-resolving technique (see Figs. 5–8). On the other hand, the nonresolving approach struggles to perform the estimation for values of Δt far from the peak of the relative Fisher information (see Figs. 5 and 7, and Fig. 3 in the main text). In this case, not only the Cramér-Rao bound diverges, yielding a low precision, but also the number of failed estimations, due to statistical fluctuations, increases.

Indeed, each attempt to estimate Δt with the nonresolving technique has a generally nonvanishing probability to fail, e.g. to yield a nonfinite estimate of the delay. This happens every time the outcome of the experiment, i.e., the number of bunching and coincidence events N_B and N_C , respectively, are not compatible with the parametrisation in Δt of the relative probabilities P_η^B and P_η^C in Eq. (C12). In fact, the global maximum of the nonresolved likelihood function

$$\mathcal{L}_{NR}(\Delta t | S_{N_\gamma}) = (P_\eta^B)^{N_B} (P_\eta^C)^{N_C} \quad (D4)$$

is achieved for

$$P_\eta^C = \frac{N_C}{N_C + N_B}, \quad P_\eta^B = \frac{N_B}{N_C + N_B}. \quad (D5)$$

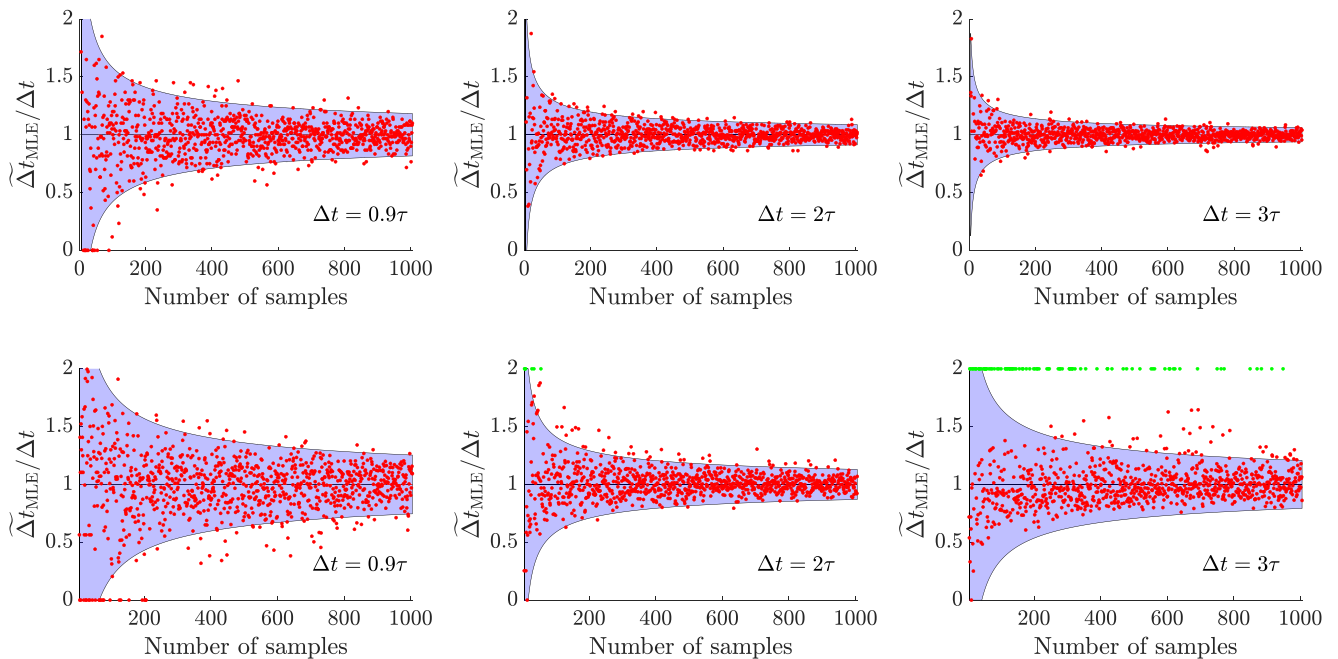


FIG. 5. Single outcomes of the estimation of the delay Δt for various number of samples, both for the frequency-resolved (upper panels) and nonresolving technique (lower panels) for three different values of the delay, for $\eta \simeq 0.8$. The area in blue between the two curves in each plot represents a range of two times the Cramér-Rao bound from the true value of the delay. We can see how the estimations concentrate much more around Δt for the frequency-resolving approach, especially for larger delays, where the nonresolving approach tends to fail. The green points in the lower panels represent failed estimations of the nonresolving technique: due to statistical fluctuations, more visible with smaller numbers of samples, it is sometimes possible to observe a counting of bunching and coincidence events not compatible with the expressions of the respective probabilities in Eq. (C12) for any finite value of Δt . These failed estimates are mostly encountered for values of the delay far from the peak of the Fisher information, but also for optimal values of the delay when the indistinguishability η at the detectors is small (see Fig. 3 in the main text).

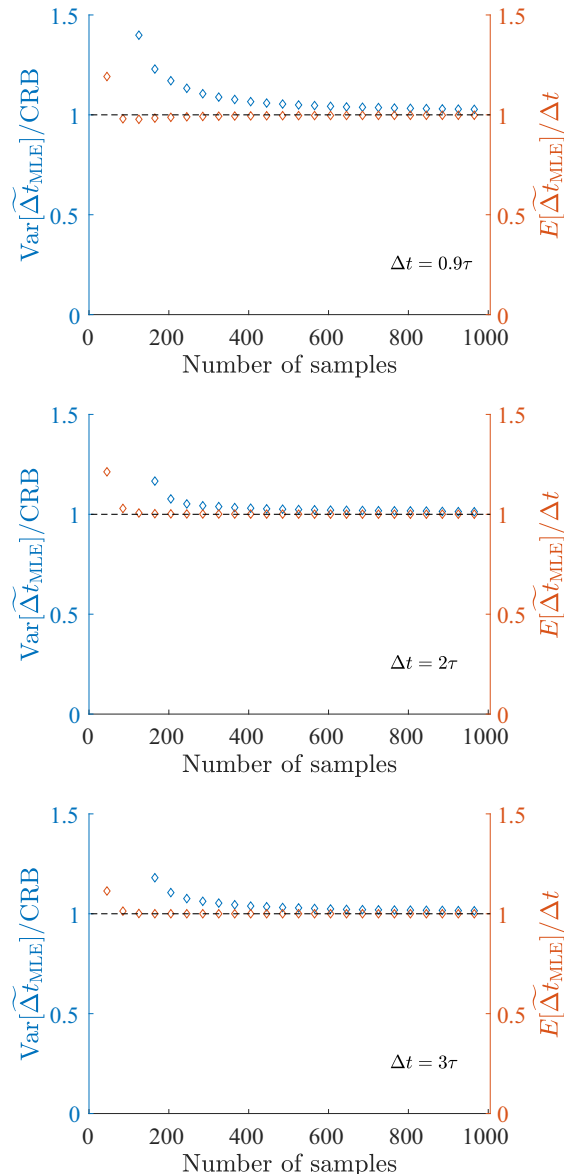


FIG. 6. Numerical simulation for the estimation of the delay with the frequency-resolving technique have been carried out, and statistical averages over 10^6 iterations of the estimation are plotted for the expectation value and the variance of the maximum-likelihood estimator, for $\eta \simeq 0.8$. Both unbiasedness and efficiency are achieved for a numbers of samples smaller than 1000.

Employing the expressions of P_η^C or P_η^B in Eq. (C12), and solving in Δt either of the conditions in Eq. (D5), one obtains an analytical expression of the maximum-likelihood estimator

$$\Delta t_{\text{NR}}(N_C, N_B) = \pm \frac{1}{\sigma} \sqrt{\log \left(\eta^2 \frac{N_B + N_C}{N_B - N_C} \right)}. \quad (\text{D6})$$

However, for certain outcomes $S_{N_\gamma} = \{N_B, N_C\}$ of the experiment, the conditions in Eq. (D5) cannot be satisfied

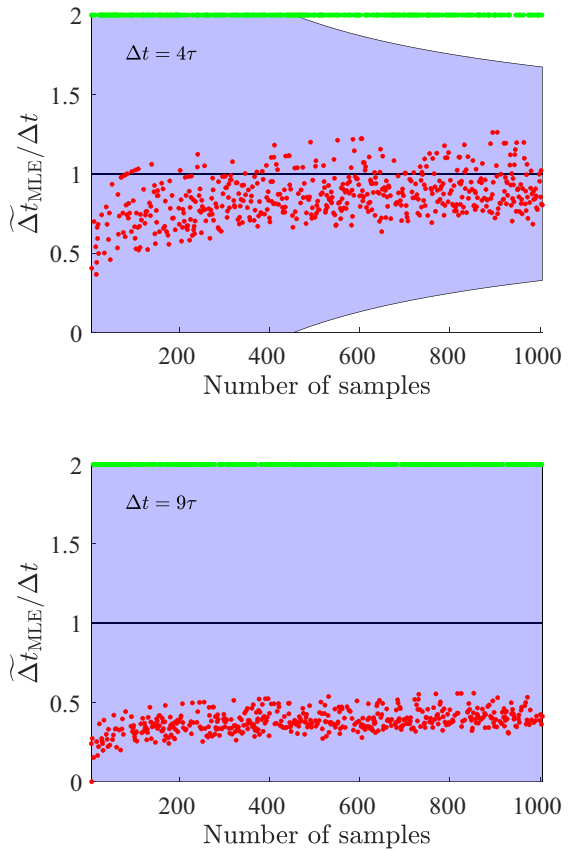


FIG. 7. Numerical simulations of the estimation for delays $\Delta t = 4\tau, 9\tau$ through the nonresolving technique, with $\eta \simeq 0.8$. In this regime, the Cramér-Rao bound drastically increases as the Fisher information in Eq. (13) decreases exponentially for increasing Δt . Moreover, many iterations fail to yield a finite estimate of the delay due to the statistical fluctuations in the number of coincidence and bunching events observed, as it can be seen from the density of green points, each one representing a failed estimation.

for any real, finite value Δt of the delay. For example, if one observes in a given experiment $N_C > N_B$, the condition in Eq. (D5) cannot be satisfied for any real Δt , since $P_\eta^B \geq P_\eta^C$ for every real, finite value of Δt [see Eq. (C12)], and indeed in this scenario the analytical estimator in Eq. (D6) yields a complex number. In this case, the real value of Δt maximizing the likelihood function in Eq. (D4) is the value for which P_η^B is the smallest and P_η^C the largest possible, i.e., $\Delta t = \infty$. The probability P_{fail} that an experiment yields a nonfinite estimate of the delay can be calculated as the sum, over all the possible values of N_C satisfying $N_C \geq N_B$ (i.e., $N_C \geq N_\gamma/2$) of the probabilities $P(N_C)$ that N_C coincidence events are observed. These probabilities follow the binomial distribution; thus, the overall probability of failure, plotted in Fig. 9, is given by

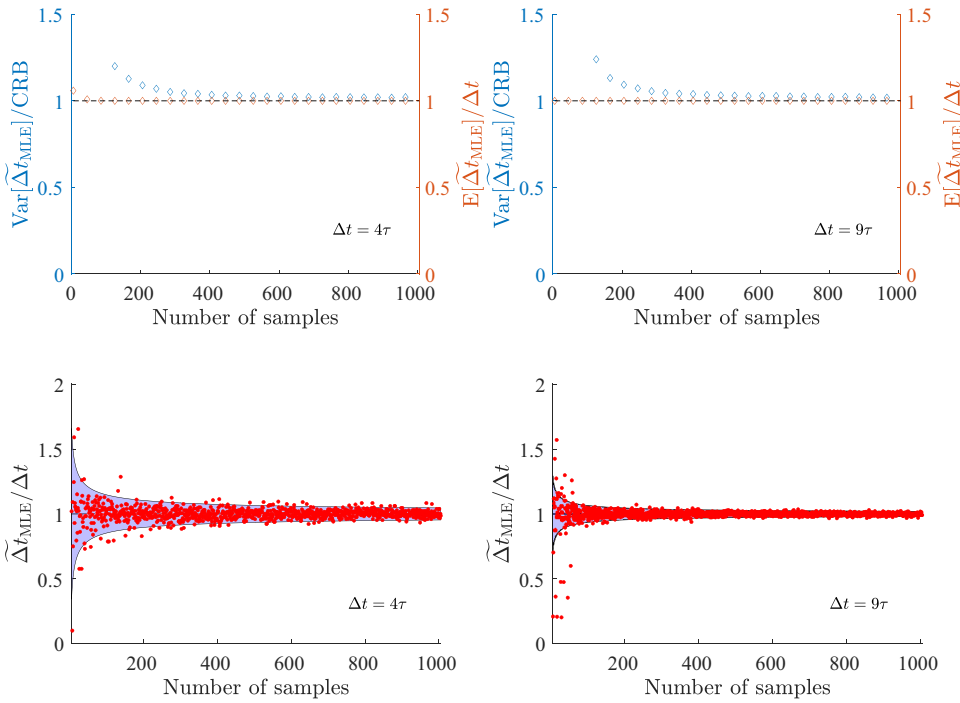


FIG. 8. Numerical simulations of the estimation for large delays through our frequency-resolving technique, with $\eta \simeq 0.8$. We can see that the unbiasedness and the saturation of the Cramér-Rao bound are effectively reached within the range of $N_\gamma = 1000$ samples observed.

$$\begin{aligned} P_{\text{fail}}(N_\gamma, \eta) &= \sum_{N_C=\lceil N_\gamma/2 \rceil}^{N_\gamma} P(N_C) \\ &= \sum_{N_C=\lceil N_\gamma/2 \rceil}^{N_\gamma} \binom{N_\gamma}{N_C} \left(\frac{1 - \eta^2 e^{-\Delta t \sigma^2}}{2} \right)^{N_C} \\ &\quad \times \left(\frac{1 + \eta^2 e^{-\Delta t \sigma^2}}{2} \right)^{N_\gamma - N_C}, \end{aligned} \quad (\text{D7})$$

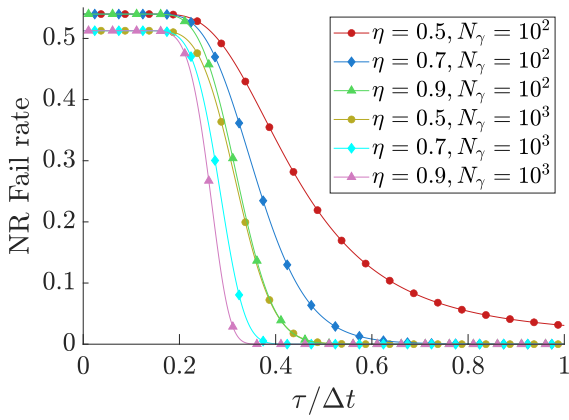


FIG. 9. Plots of P_{fail} in Eq. (D7) as a function of $\tau/\Delta t$. Differently from our frequency-resolving technique, the fail rate of the nonresolving approach drastically increases either for smaller values of $\tau/\Delta t$ or for small values of η for any value of $\tau/\Delta t$, including the optimal scenarios $\Delta t \simeq 2\tau$ (see Fig. 2).

where $\binom{k}{n} = n!/[k!(n-k)!]$ is the binomial coefficient, while $\lceil x \rceil$ denote the closest integer to x rounded up.

-
- [1] C. K. Hong, Z. Y. Ou, and L. Mandel, Measurement of Subpicosecond Time Intervals between Two Photons by Interference, *Phys. Rev. Lett.* **59**, 2044 (1987).
 - [2] Y. H. Shih and C. O. Alley, New Type of Einstein-Podolsky-Rosen-Bohm Experiment Using Pairs of Light Quanta Produced by Optical Parametric Down Conversion, *Phys. Rev. Lett.* **61**, 2921 (1988).
 - [3] I. Abram, R. K. Raj, J. L. Oudar, and G. Dolique, Direct Observation of the Second-Order Coherence of Parametrically Generated Light, *Phys. Rev. Lett.* **57**, 2516 (1986).
 - [4] Sudhakar Prasad, Marlan O. Scully, and Werner Martienssen, A quantum description of the beam splitter, *Opt. Commun.* **62**, 139 (1987).
 - [5] Z. Y. Ou, C. K. Hong, and L. Mandel, Relation between input and output states for a beam splitter, *Opt. Commun.* **63**, 118 (1987).
 - [6] H. Fearn and R. Loudon, Quantum theory of the lossless beam splitter, *Opt. Commun.* **64**, 485 (1987).
 - [7] J. G. Rarity and P. R. Tapster, Fourth-order interference in parametric downconversion, *J. Opt. Soc. Am. B* **6**, 1221 (1989).
 - [8] Frédéric Bouchard, Alicia Sit, Yingwen Zhang, Robert Fickler, Filippo M. Miatto, Yuan Yao, Fabio Sciarrino, and Ebrahim Karimi, Two-photon interference: The Hong-Ou-Mandel effect, *Rep. Prog. Phys.* **84**, 012402 (2021).
 - [9] Ashley Lyons, George C. Knee, Eliot Bolduc, Thomas Roger, Jonathan Leach, Erik M. Gauger, and Daniele

- Faccio, Attosecond-resolution Hong-Ou-Mandel interferometry, *Sci. Adv.* **4**, 5 (2018).
- [10] Yuanyuan Chen, Matthias Fink, Fabian Steinlechner, Juan P. Torres, and Rupert Ursin, Hong-Ou-Mandel interferometry on a biphoton beat note, *npj Quantum Inf.* **5**, 43 (2019).
- [11] N. Fabre and S. Felicetti, Parameter estimation of time and frequency shifts with generalized Hong-Ou-Mandel interferometry, *Phys. Rev. A* **104**, 022208 (2021).
- [12] Natapon Harnchaiwat, Feng Zhu, Niclas Westerberg, Erik Gauger, and Jonathan Leach, Tracking the polarisation state of light via Hong-Ou-Mandel interferometry, *Opt. Express* **28**, 2210 (2020).
- [13] Harald Cramér, *Mathematical Methods of Statistics* (Princeton University Press, Princeton, 1999), Vol. 9.
- [14] Vijay K. Rohatgi and A. K. Md. Ehsanes Saleh, *An Introduction to Probability and Statistics* (John Wiley & Sons, Agawam, 2000).
- [15] Hamish Scott, Dominic Branford, Niclas Westerberg, Jonathan Leach, and Erik M. Gauger, Beyond coincidence in Hong-Ou-Mandel interferometry, *Phys. Rev. A* **102**, 033714 (2020).
- [16] T. Legero, T. Wilk, A. Kuhn, and G. Rempe, Time-resolved two-photon quantum interference, *Appl. Phys. B* **77**, 797 (2003).
- [17] Thomas Legero, Tatjana Wilk, Markus Hennrich, Gerhard Rempe, and Axel Kuhn, Quantum Beat of Two Single Photons, *Phys. Rev. Lett.* **93**, 070503 (2004).
- [18] Vincenzo Tamma and Simon Laibacher, Multiboson Correlation Interferometry with Arbitrary Single-Photon Pure States, *Phys. Rev. Lett.* **114**, 243601 (2015).
- [19] Xu-Jie Wang, Bo Jing, Peng-Fei Sun, Chao-Wei Yang, Yong Yu, Vincenzo Tamma, Xiao-Hui Bao, and Jian-Wei Pan, Experimental Time-Resolved Interference with Multiple Photons of Different Colors, *Phys. Rev. Lett.* **121**, 080501 (2018).
- [20] Vindhya Prakash, Aleksandra Sierant, and Morgan W. Mitchell, Autoheterodyne Characterization of Narrow-Band Photon Pairs, *Phys. Rev. Lett.* **127**, 043601 (2021).
- [21] Rui-Bo Jin, Thomas Gerrits, Mikio Fujiwara, Ryota Wakabayashi, Taro Yamashita, Shigehito Miki, Hirotaka Terai, Ryosuke Shimizu, Masahiro Takeoka, and Masahide Sasaki, Spectrally resolved Hong-Ou-Mandel interference between independent photon sources, *Opt. Express* **23**, 28836 (2015).
- [22] Pablo Yepiz-Graciano, Alí Michel Angulo Martínez, Dorilán Lopez-Mago, Hector Cruz-Ramirez, and Alfred B. U'Ren, Spectrally resolved Hong-Ou-Mandel interferometry for quantum-optical coherence tomography, *Photon. Res.* **8**, 1023 (2020).
- [23] T. Hiemstra, T. F. Parker, P. Humphreys, J. Tiedau, M. Beck, M. Karpiński, B. J. Smith, A. Eckstein, W. S. Kolthammer, and I. A. Walmsley, Pure Single Photons from Scalable Frequency Multiplexing, *Phys. Rev. Appl.* **14**, 014052 (2020).
- [24] Simon Laibacher and Vincenzo Tamma, Symmetries and entanglement features of inner-mode-resolved correlations of interfering nonidentical photons, *Phys. Rev. A* **98**, 053829 (2018).
- [25] Venkata Vikram Orre, Elizabeth A. Goldschmidt, Abhinav Deshpande, Alexey V. Gorshkov, Vincenzo Tamma, Mohammad Hafezi, and Sunil Mittal, Interference of Temporally Distinguishable Photons using Frequency-Resolved Detection, *Phys. Rev. Lett.* **123**, 123603 (2019).
- [26] Simon Laibacher and Vincenzo Tamma, From the Physics to the Computational Complexity of Multiboson Correlation Interference, *Phys. Rev. Lett.* **115**, 243605 (2015).
- [27] Vincenzo Tamma and Simon Laibacher, Multi-boson correlation sampling, *Quantum Inf. Process.* **15**, 1241 (2016).
- [28] Vincenzo Tamma and Simon Laibacher, Scattershot multiboson correlation sampling with random photonic inner-mode multiplexing, arXiv:1801.03832.
- [29] Carl W. Helstrom, Quantum detection and estimation theory, *J. Stat. Phys.* **1**, 231 (1969).
- [30] A. S. Holevo, *Probabilistic and Statistical Aspects of Quantum Theory*, Publications of the Scuola Normale Superiore (Scuola Normale Superiore, 2011).
- [31] Kyle M. Jordan, Raphael A. Abraham, and Jeff S. Lundeen, Quantum metrology timing limits of the Hong-Ou-Mandel interferometer and of general two-photon measurements, *Phys. Rev. A* **106**, 063715 (2022).
- [32] Peter J. Mosley, Jeff S. Lundeen, Brian J. Smith, Piotr Wasylczyk, Alfred B. U'Ren, Christine Silberhorn, and Ian A. Walmsley, Heralded Generation of Ultrafast Single Photons in Pure Quantum States, *Phys. Rev. Lett.* **100**, 133601 (2008).
- [33] Magued B. Nasr, Silvia Carrasco, Bahaa E. A. Saleh, Alexander V. Sergienko, Malvin C. Teich, Juan P. Torres, Lluis Torner, David S. Hum, and Martin M. Fejer, Ultra-broadband Biphotons Generated via Chirped Quasi-Phase-Matched Optical Parametric Down-Conversion, *Phys. Rev. Lett.* **100**, 183601 (2008).
- [34] Silke Aumann, Sabine Donner, Jörg Fischer, Frank Müller, in *High Resolution Imaging in Microscopy and Ophthalmology: New Frontiers in Biomedical Optics*, edited by Josef F. Bille (Springer International Publishing, Cham, 2019), pp. 59–85.
- [35] Thang L. Nguyen, Soorya Pradeep, Robert L. Judson-Torres, Jason Reed, Michael A. Teitel, and Thomas A. Zangle, Quantitative phase imaging: Recent advances and expanding potential in biomedicine, *ACS Nano* **16**, 11516 (2022).
- [36] Tatyana Tishko, Tishko Dmitry, and Titar Vladimir, *Holographic Microscopy of Phase Microscopic Objects* (World Scientific, Singapore, 2011).
- [37] Wolfgang Drexler, Uwe Morgner, Ravi K. Ghanta, Franz X. Kärtner, Joel S. Schuman, and James G. Fujimoto, Ultrahigh-resolution ophthalmic optical coherence tomography, *Nat. Med.* **7**, 502 (2001).
- [38] YongKeun Park, Christian Depeursinge, and Gabriel Popescu, Quantitative phase imaging in biomedicine, *Nat. Photonics* **12**, 578 (2018).
- [39] Simo Saarakkala, Shu-Zhe Wang, Yan-Ping Huang, and Yong-Ping Zheng, Quantification of the optical surface reflection and surface roughness of articular cartilage using optical coherence tomography, *Phys. Med. Biol.* **54**, 6837 (2009).
- [40] Matteo G. A. Paris, Quantum estimation for quantum technology, *Int. J. Quantum Inf.* **7**, 125 (2009).